Wheat 2-Cys peroxiredoxin plays a dual role in chlorophyll biosynthesis and adaptation to high temperature

Divya Mishra (iD), **Shubhendu Shekhar, Subhra Chakraborty** (iD) **and Niranjan Chakraborty**[*] (iD)

National Institute of Plant Genome Research, Jawaharlal Nehru University Campus, Aruna Asaf Ali Marg, New Delhi 110067, India

SUMMARY

The molecular mechanism of high-temperature stress (HTS) response, in plants, has so far been investigated using transcriptomics, while the dynamics of HTS-responsive proteome remain unexplored. We examined the adaptive responses of the resilient wheat cultivar 'Unnat Halna' and dissected the HTS-responsive proteome landscape. This led to the identification of 55 HTS-responsive proteins (HRPs), which are predominantly involved in metabolism and defense pathways. Interestingly, HRPs included a 2-cysteine peroxiredoxin (2CP), designated Ta2CP, presumably involved in stress perception and adaptation. Complementation of *Ta2CP* in yeast and heterologous expression in Arabidopsis demonstrated its role in thermotolerance. Both *Ta2CP* silencing and overexpression inferred the involvement of Ta2CP in plant growth and chlorophyll biosynthesis. We demonstrated that Ta2CP interacts with protochlorophyllide reductase b, TaPORB. Reduced *TaPORB* expression was found in Ta2cp-silenced plants, while upregulation was observed in Ta2CP-overexpressed plants. Furthermore, the downregulation of Ta2CP in Taporb-silenced plants and reduction of protochlorophyllide in Ta2cp-silenced plants suggested the key role of Ta2CP in chlorophyll metabolism. Additionally, the transcript levels of *AGPase1* and starch were increased in Ta2cp-silenced plants. More significantly, HTS-treated Ta2cp-silenced plants showed adaptive responses despite increased reactive oxygen species and peroxide concentrations, which might help in rapid induction of high-temperature acclimation.

Keywords: antioxidant defense, bread wheat, cell death suppressors, cytoplasmic proteome, high-temperature stress, stress-adaptive responses, thermotolerance.

INTRODUCTION

High-temperature stress (HTS) is a major threat to plant survival and cause of crop losses worldwide, posing major challenges to global food security. Recently, the Paris Agreement on global warming concluded a 1°C increase above the pre-industrial level has already been reached, and an additional increase of 0.5°C is expected by 2050. Notably, the temperature of several regions of India has already been increased by 1.2°C above the pre-industrial level as against 1°C in other countries, which is a major concern. Given the trend of rising temperatures, many parts of the world, including India, are likely to have adverse impacts caused by global warming, which will ultimately lead to food scarcity (IPCC, 2018). Bread wheat is a winter-seasoned crop that is highly vulnerable to changes in temperature (Chauhan *et al.*, 2011). It is the dominant crop across geographic regions, and is used for human food and livestock feed. The increase of 1°C in temperature can hamper wheat production by 6% (Asseng *et al.*, 2014).

The success of wheat production largely depends on stress adaptability, especially against HTS, and the potential to have yield improved.

Plants, as sessile organisms, have evolved strategies and high plasticity to endure and adapt to non-ambient temperatures. These adaptive strategies impact on all cellular functions and play critical roles in metabolic regulation through an array of signaling cascades at the organellar level. Until recently, transcriptome-based analysis has been the mainstream tool to understand the molecular mechanism of HTS responses and cellular adaptation (Shi *et al.*, 2017; Liu *et al.*, 2020). However, dissection of the proteome dynamics of HTS-induced responses is imperative to determine thermotolerance. The cytoplasm of the plant cell serves as the intracellular matrix that harbors most subcellular organelles, except the nucleus (Streward, 1942). More significantly, mRNA abundance and rate of protein synthesis suggest that the regulation of gene expression mainly occurs in the cytoplasm, not in the nucleus (Schwanhäusser *et al.*, 2011). Therefore, it is

important to examine the cytoplasmic proteome landscape, which would help on efficiently identifying the key factors associated with thermotolerance acquisition in plants.

The present study was designed as a comparative proteomics of the cytoplasm of a thermotolerant wheat cultivar, U. Halna. The proteomic analysis led to the identification of a number of HTS-responsive proteins (HRPs), presumably involved in acclimation to high temperatures. Screening of cytoplasmic signature proteins led us to a 2-cysteine peroxiredoxin, hereafter designated Ta2CP, which was chosen for detailed characterization to evaluate its role in stress tolerance. The 2CPs belong to the peroxiredoxin (Prx) family of proteins involved in the detoxification of alkyl and hydrogen peroxide (Horling *et al.*, 2002; König *et al.*, 2002; Broin and Rey, 2003; Awad *et al.*, 2015). The Prxs have been a major focus of plant stress adaptation studies, especially in the past few decades. The 2CPs have been suggested to be integrated into chloroplasts from cyanobacteria during the process of evolution (Weber and Osteryoung, 2010). Previous studies clearly established that 2CPs play a key role in the maintenance of reactive oxygen species (ROS) homeostasis and regulate the chloroplast metabolism (König *et al.*, 2002; Pulido *et al.*, 2010; Vaseghi *et al.*, 2018). The plastid-localized 2CP interacts with thylakoid APx to protect the photosynthetic apparatus through maintenance of the water−water cycle (Awad *et al.*, 2015). Additionally, 2CP maintains the electron pool of the photosystem by accepting reducing equivalents from ferredoxin-ferredoxin/thioredoxin reductase-thioredoxin (Fd-FTR-Trx) and NADP-thioredoxin reductase C (NTRC; Kirchsteiger *et al.*, 2009; Pulido *et al.*, 2010; Awad *et al.*, 2015; Cheng *et al.*, 2016). In plants, 2CP has the ability to change structural conformation and functions as a chaperone (Jang *et al.*, 2004; Kim *et al.*, 2008; Cerveau *et al.*, 2019). However, it is not clearly understood how 2CP participates in chlorophyll metabolism, thereby affecting photosynthesis and sugar−starch homeostasis. Although 2CP has been linked to abiotic stress responses (Vidigal *et al.*, 2014), the role of 2CP in thermotolerance is largely unknown.

To reveal the physiological functions of Ta2CP, we investigated how Ta2CP affects the photosynthetic machinery, with specific emphasis on chlorophyll synthesis and peroxidase status, and how it influences sugar−starch homeostasis. The results indicate that silencing of Ta2CP leads to HTS-induced higher accumulation of ROS, orchestrating cell apoptosis. However, tight regulation of Ta2CP induces the activation of cell defense pathway, tandemly working with autophagy machinery, and acts as a safeguard against HTS-induced cell death. Together, these results suggest that Ta2CP is a HTS-sensitive antioxidant that plays an important role in thermotolerance.

RESULTS

HTS-mediated morphophysiological alterations in wheat

The degree of thermotolerance and adaptive physiological responses of U. Halna were evaluated. Seedlings showed leaf-rolling and yellowing at advanced stages (d-3 and d-4) of the HTS (Figure S1a,b). Furthermore, we examined H_2O_2 abundance, and cell viability against H_2O_2 toxicity. An increase in H_2O_2 levels and cell death was observed in later stages d-3 and d-4, respectively (Figure S1c–f). A considerable decrease was found in antioxidant enzyme activity in the later stages. A decrease in the activity of ascorbate peroxidase, glutathione reductase and superoxide dismutase was observed in d-4, while peroxidase activity was decreased in d-3 (Figure S1g–j). We observed the accumulation of soluble sugars during HTS, which functions as osmoprotectant (Figure S1k). Furthermore, ultrastructural analysis revealed deformation in the cell shape (Figure S1l–I, II), along with unstacking of chloroplast grana and mitochondrial cristae in d-4 when compared with unstressed control (Figure S1l-III−VI).

Proteometabolomic response of wheat exposed to HTS

The cytoplasm is the intracellular matrix, which interconnects metabolic networks, and we sought to investigate the effects of HTS on the cytoplasmic proteome. The cytoplasmic proteins were isolated, and its enrichment was checked by the presence of organelle-specific markers (Figure S2a–d). The abundance of cytochrome c oxidase, RuBisCO L subunit, fructose-1,6-biphosphate aldolase and the absence of both xyloglucan endo-transglycosylase and anti-plasma membrane intrinsic protein 2 in the fraction indicated the enrichment of cytoplasmic proteins (Figure S2b). The enriched fraction exhibited the activity of alcohol dehydrogenase, further confirming the abundance of cytoplasmic proteins (Figure S2c). The HTS-responsive cytoplasmic proteome was investigated by 2-DE and statistically analyzed by PDQuest software (Figures S3 and S4), and the proteins were identified by LC-MS/MS analysis. In all, 55 differentially expressed proteins were identified, referred to as HRPs, of which 10 proteins were upregulated and 29 were downregulated, while 16 proteins showed mixed expression patterns (Figures 1a and S5; Tables S1 and S2). The interaction network revealed that HRPs associated with carbohydrate metabolic pathways interact with proteins of redox homeostasis, chaperone machinery and photosynthetic pathways (Figure 1b; Table S3). Principal component analysis (PCA) revealed that few HRPs associated with photosynthesis and redox homeostasis were significantly altered during HTS (Figure 1c). Furthermore, to better understand the HTS-modulated metabolic changes, the metabolite profiles were compared in d-4 with the unstressed control. Differential abundance was observed in 33 non-redundant metabolites, albeit some of the
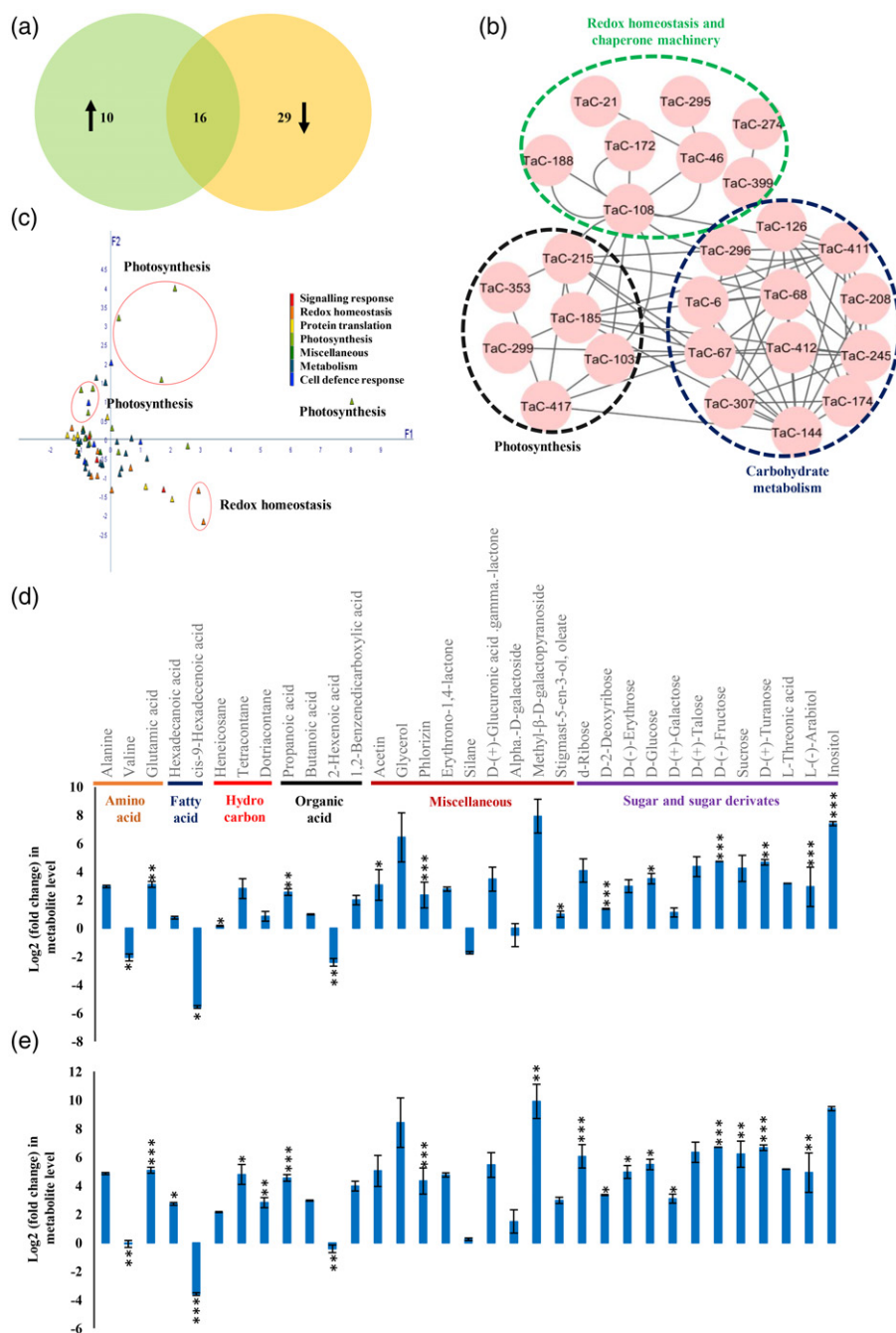
Figure 1. High-temperature stress (HTS)-induced proteometabolomic shift in thermotolerant wheat.
(a) Venn diagram showing the number of HTS-induced upregulated and downregulated proteins along with those exhibiting mixed pattern of expression.
(b) Interaction network of HTS-responsive proteins (HRPs) and HRPs belonging to different pathways are encircled by dotted lines in different colors.
(c) Principal component analysis (PCA) on protein fold change value showing HRPs associated with photosynthesis and redox homeostasis were significantly affected. Colors of different triangles on PCA plot represent the functional classes, and circles represent the protein clusters.
(d,e) Bar graphs depicting log2 fold change values of differentially accumulated metabolites in d-4 relative to UC. The experiments were performed in three replicates with two internal standard controls: (d) 2-methyl-3-heptanone and (e) D-ribitol. Metabolites marked with ***$P < 0.001$, **$P < 0.01$ and *$P < 0.05$ were significantly different (Student's *t*-test). The metabolites were categorized in different functional classes, as indicated.

metabolites were exclusively accumulated in either unstressed control or d-4 (Figure 1d,e; Table S4). Interestingly, sugars and their derivatives showed an increased accumulation, indicating a major shift in sugar metabolism under HTS, which substantiated previous observations of HTS-induced accumulation of soluble sugars during the

advanced stage (Figure S1e). A shift toward sugar metabolism and accumulation of different amino acids under HTS also suggests an intimate association of carbohydrate and amino acid metabolic pathways for the alleviation of HTS and, based on these findings, a HTS-responsive network in wheat has been postulated (Figure S6).

Proteomic identification of HTS-responsive Ta2CP

Screening for potential target/s in HTS-responsive proteome led to the identification of a Ta2CP that showed increased expression, particularly at d-4 (Figure 2a,b). The increase in *Ta2CP* transcript was also seen in d-3 of HTS, which further declined at d-4 (Figure 2c). Arabidopsis homologs of five HRPs reported as the interactor of At2CP (Muthuramalingam *et al.*, 2009; Cerveau *et al.*, 2016) further indicated that Ta2CP possibly interacts with these HRPs and plays a crucial role in HTS-responsive metabolic pathways (Figure S7a; Table S5). Previous findings have shown more than one isoform of 2CP in Arabidopsis and rice (Dietz, 2011). As 2CP belongs to the Prx family, we investigated the distribution of Prx along with 2CP in major evolutionary lineages of the plant kingdom. The members of the Prx family appeared to be the highest in wheat possibly due to the hexaploid genome, albeit only one type of 2CP was found (Figure S7b,c; Table S6).

or the experimental validation of the subcellular localization, we isolated the chloroplast fraction and examined the presence of Ta2CP along with chloroplast-specific markers, light harvesting complex, RuBisCO L subunit, and mitochondrial-specific marker cytochrome c oxidase. When compared with the whole-cell extract, abundance of Ta2CP was found to be in the chloroplast-enriched fraction, further corroborating its localization in chloroplast (Figure 2d).

Heterologous complementation of Ta2CP in yeast mutants and overexpression of Ta2CP in Arabidopsis

Thiol-specific antioxidant proteins (TSA1 and TSA2) are plant 2CP homologs in yeast and are involved in redox homeostasis (Liebthal *et al.*, 2018). Disruption of TSA1/TSA2, independently or simultaneously, has been shown to cause growth defects in yeast (Wong *et al.*, 2004). To ascertain the functional role of Ta2CP, we complemented the single mutants *Δtsa1* and *Δtsa2*, and double mutant *Δtsa1Δtsa2* in yeast with pYES-DEST52:*Ta2CP*. The *Δtsa1Δtsa2* double mutant showed a severe growth defect followed by *Δtsa1* compared with *Δtsa2*. Importantly, the complemented lines (*Δtsa1:Ta2CP*, *Δtsa2:Ta2CP* and *Δtsa1Δtsa2:Ta2CP*) exhibited better phenotype compared with their mutants under unstressed conditions (Figure 2e). Functional complementation and rescue of growth defects in *Δtsa1Δtsa2:Ta2CP* were observed under high and low temperature, hypersalinity, osmotic and oxidative stress (Figure 2f–j). In summary, the results confirm the

ability of Ta2CP to complement the function of yeast TSA and provide multi-stress tolerance (Figure 2e–j).

Further investigations of Ta2CP-overexpressed Arabidopsis plants displayed green and healthy phenotypes in unstressed (Figure 2k) and HTS conditions (Figure 2l), suggesting a role of Ta2CP in thermotolerance in the overexpression lines when compared with wild-type ecotype Col-0. Altogether, these results suggest a cross-kingdom adaptive response of Ta2CP.

Role of Ta2CP in plant development and thermotolerance

To define the role of Ta2CP, tobacco rattle virus (TRV)-based virus-induced gene silencing (VIGS) was employed to knockdown Ta2CP in wheat (Figure S8a). The expression of Ta2CP was significantly reduced in Ta2cp-silenced plants (Figure S8b), which resulted in a photobleaching-like phenotype, impaired leaf morphology and reduced plant height (Figures 3a, upper panel, and S8a–d). Ta2CP knockdown plants exhibited compromised defense when exposed to HTS conditions (Figure 3a, lower panel). To express Ta2CP in wheat, the vacuum-assisted *Agrobacterium* transformation method was used to produce the Ta2CP-overexpressed plants using pEarleyGate101, along with pBI121 harboring *GUS* reporter gene as a positive control (Figure S9a,b). In contrast to silenced plants, Ta2CP-overexpressed plants exhibited much better growth and development with increased Ta2CP expression (Figures 3b, upper panel, and S9c,d). To decipher the role of Ta2CP in thermotolerance, Ta2cp-silenced and Ta2CP-overexpressed plants were exposed to HTS conditions. While Ta2cp-silenced plants exhibited extensive leaf curling and wilting, the Ta2CP-overexpressed plants were better adapted in HTS conditions (Figure 3a,b, lower panel). Further analysis of the role of Ta2CP in chlorophyll metabolism revealed a significant reduction in chlorophyll in Ta2cp-silenced plants, especially chlorophyll a under high-temperature conditions, which was in agreement with the photobleaching-like phenotype (Figure 3c,d). Significantly, Ta2CP-overexpressed plants showed higher chlorophyll a and b content than the vector-transformed plants. Notably, HTS-induced increase was observed only in chlorophyll a, while no significant effect was observed on chlorophyll b in Ta2CP-overexpressed plants (Figure 3e,f).

Ta2CP interacts with TaPORB and participates in chlorophyll biosynthesis

The difference in chlorophyll content between Ta2cp-silenced and overexpressed plants necessitated to dissect the role of Ta2CP in chlorophyll biosynthesis and to acknowledge the interacting partners falling together in the pathway. Previous co-immunoprecipitation study in *Arabidopsis* has dissected putative interactors of At2CP, including chlorophyll biosynthetic pathway (Cerveau *et al.*,
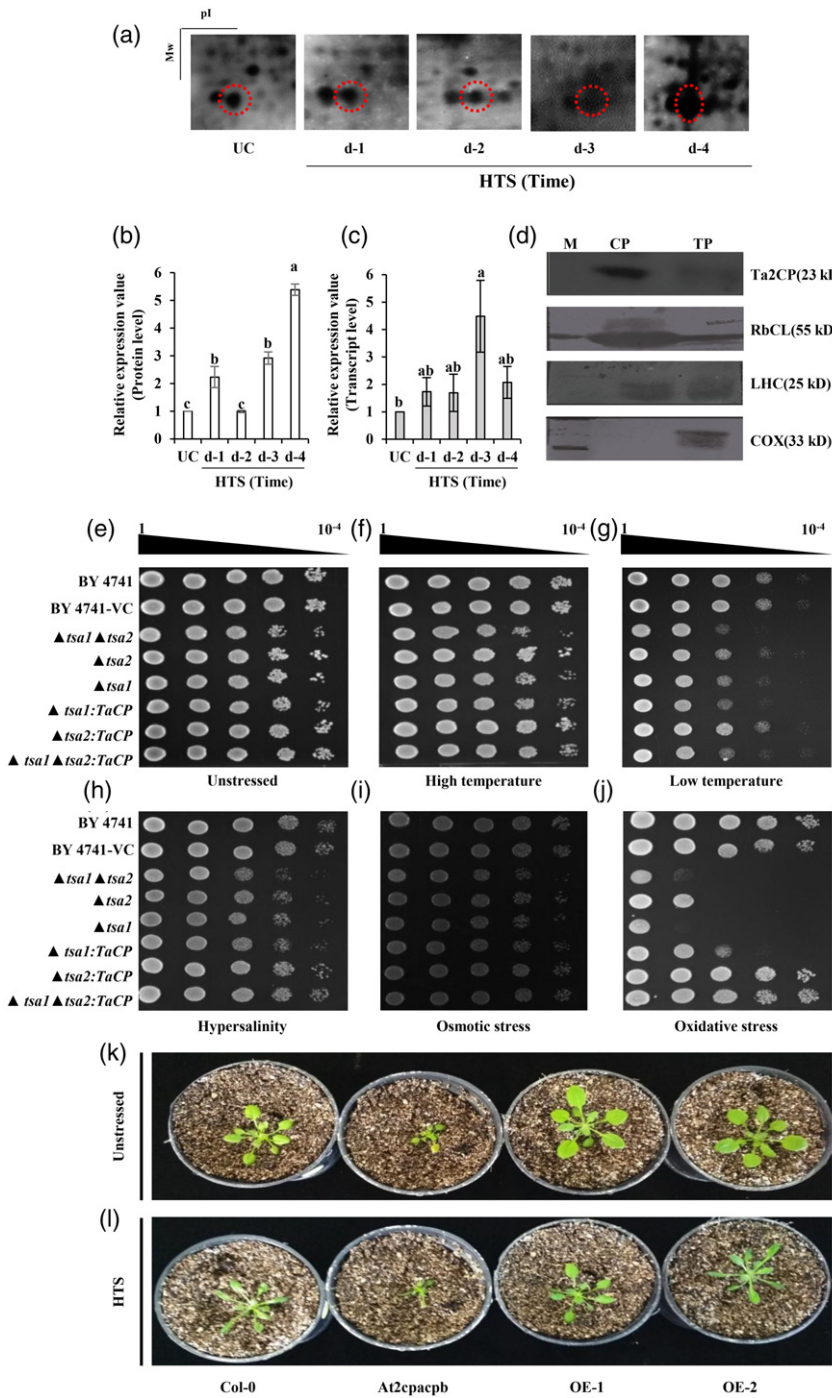
Figure 2. Proteomic identification and functional annotation of high-temperature stress (HTS)-responsive candidate, Ta2CP.

(a) Magnified image of 2-DE gels (gel images shown in Figure S3a) displaying HTS-induced differential expression of Ta2CP.

(b,c) Bar graphs represent HTS-induced changes in expression values (b) at protein level (computed through the raw 2-DE gels images) and (c) transcript abundance. Values represent means ± SE, and bars with different letters are significantly different [$P < 0.05$, Fisher's least significant difference (LSD)].

(d) Immunoblots showing relative abundance of Ta2CP, RbCL, LHC and COX in chloroplast fraction and whole cell extract. M, marker; CP, chloroplast; TP, total protein; 2CP, 2-cysteine peroxiredoxin; RbCL, RuBisCO L subunit; LHC, light harvesting complex; COX, cytochrome c oxidase.

(e–j) Growth phenotypes of BY4741, BY4741-VC, *Δtsa1Δtsa2*, *Δtsa2*, *Δtsa1*, *Δtsa1:Ta2CP*, *Δtsa2:Ta2CP* and *Δtsa1Δtsa2:Ta2CP* yeast strains (e) unstressed, (f) high-temperature and (g) low-temperature stress, (h) hypersalinity), (i) osmotic stress and (j) oxidative stress.

(k,l) Phenotypes of wild-type Arabidopsis Col-0, double mutant (*At2cpacpb*) and Ta2CP-overexpressed (OE-1 and OE-2) Arabidopsis plants under unstressed and HTS conditions. The experiments were carried out in triplicate (*n* = 3).

2016). To gain more insight into the effect of Ta2CP on chlorophyll biosynthesis, we examined its putative interaction partners, particularly glutamate-1-semialdehyde-2,1-aminomutase (GSA), protochlorophyllide reductase B (PORB) and coproporphyrinogen-III oxidase (CPO). As a first step in recognizing the relationship between the putative partners and Ta2CP, the relative abundance of their transcripts was quantified in Ta2cp-silenced and Ta2CP-overexpressed plants. The transcript reduction of PORB in Ta2cp-silenced plants but enhancement in Ta2CP-overexpressed plants demonstrated a proof-of-concept for the photobleaching-like phenotype of Ta2cp-silenced plants (Figure 4a,b). Additionally, TaCPO showed increased expression in Ta2CP-overexpressed plants, while no effect was seen in Ta2cp-silenced plants (Figure S10a,b). Furthermore, the transcript abundance of *GSA* in Ta2cp-silenced or Ta2CP-overexpressed plants showed no correlation (Figure S10c,d).
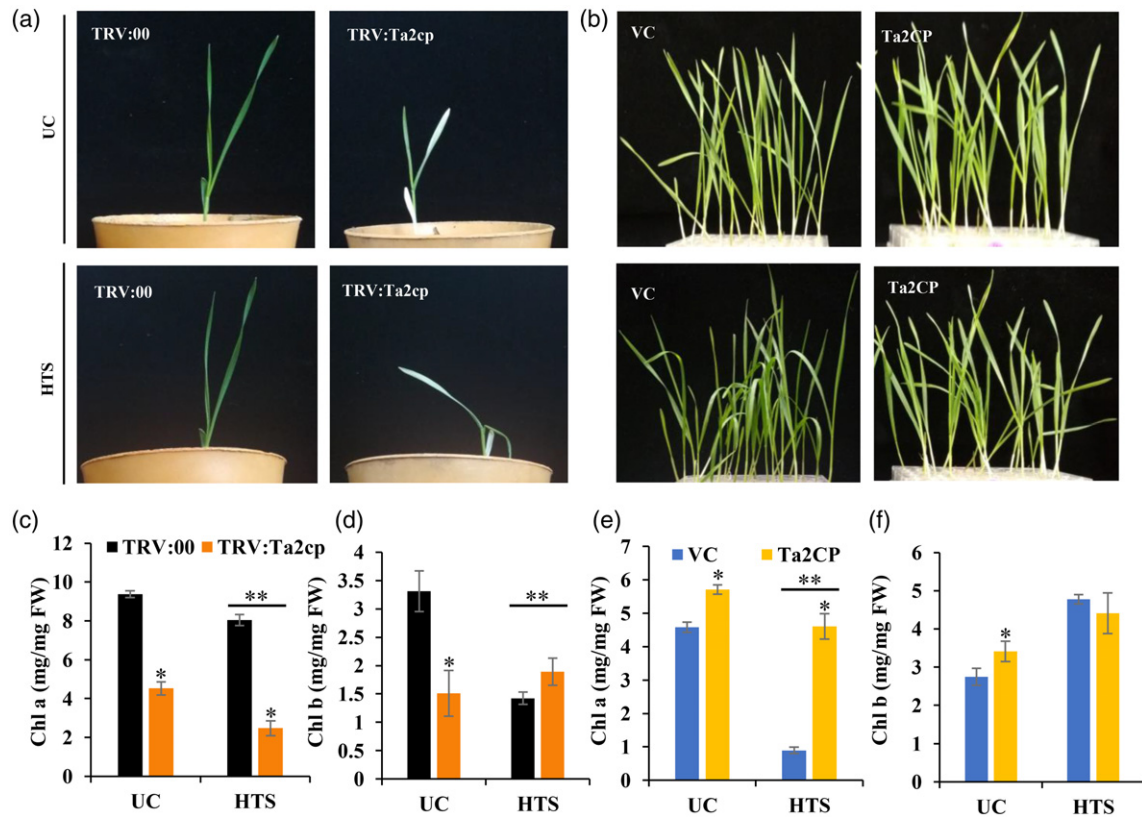
Figure 3. Role of Ta2CP in growth and development of wheat.
(a) The images showing phenotypic changes in silenced Ta2cp (TRV:Ta2cp) compared with the vector control (VC; TRV:00) plants under unstressed (upper panel) and high-temperature stress (HTS) conditions (lower panel).
(b) Transient expression of Ta2CP in wheat along with their VC under unstressed (upper panel) and HTS-treated conditions (lower panel).
(c–f) Bar graphs showing alterations in chlorophyll a and chlorophyll b content in (c, d) Ta2cp-silenced and (e,f) Ta2CP-overexpressed plants with their respective controls TRV:00 and VC, under unstressed and HTS conditions, respectively.
Data shown are the means ± SE of three experiments. Single asterisk denotes statistical significance relative to their corresponding TRV:00/VC (Student's *t*-test), while double asterisks denote significant differences between TRV:00/VC and silenced/overexpressed plants (two-way ANOVA) challenged with HTS ($P < 0.05$).

Next, we sought to determine whether Ta2CP interacts with the candidate partners TaGSA, TaPORB and TaCPO using the yeast-2-hybrid (Y2H) assay. The results indicate that Ta2CP physically interacts with TaPORB (Figure 4c). The interaction was further confirmed by *in planta* bimolecular fluorescence complementation (BiFC) analysis with Ta2CP fused at the N-terminal and TaPORB at the C-terminal of the YFP-BiFC vector as detailed later in the Experimental Procedures section. Co-expression of TaPORB-YFPc and Ta2CP-YFPn resulted in bright YFP fluorescence in the chloroplast, indicating an interaction between Ta2CP and TaPORB (Figure 4d). However, no fluorescence was observed when leaves were co-transformed with TaPORB-YFPc and YFPn or with Ta2CP-YFPn and YFPc.

To further explore the role of Ta2CP in photosynthesis and the relationship between Ta2CP and TaPORB, TaPORB was silenced in wheat. The Taporb-silenced plants showed stunted growth and a pale-green phenotype with significantly reduced *TaPORB* expression compared with the

vector control (TRV:00; Figure 4e,f). Interestingly, silencing *TaPORB* resulted in reduced levels of *Ta2CP* transcripts, showing correlation with the observed downregulation of *PORB* in *Ta*2cp-silenced plants (Figure 4a,f). These findings prompted us to determine the protochlorophyllide content, which revealed a reduction in both Taporb- and Ta2cp-silenced plants as compared with TRV:00 plants (Figure 4g). This substantiates earlier results that led to the conclusion that downregulation of PORB/*fgl* causes lower accumulation of protochlorophyllide (Sakuraba *et al.*, 2013). These results suggest that Ta2CP functions synergistically with TaPORB in the conversion of protochlorophyllide to chlorophyll a, and plays a crucial role in chlorophyll biosynthesis.

Ta2CP-mediated effect on starch biosynthesis

Plants accumulate starch as both transient and long-term carbohydrate reserves, which maintains carbon supply in response to multiple physiological demands, including stress responses. Starch accumulation in plants is critically
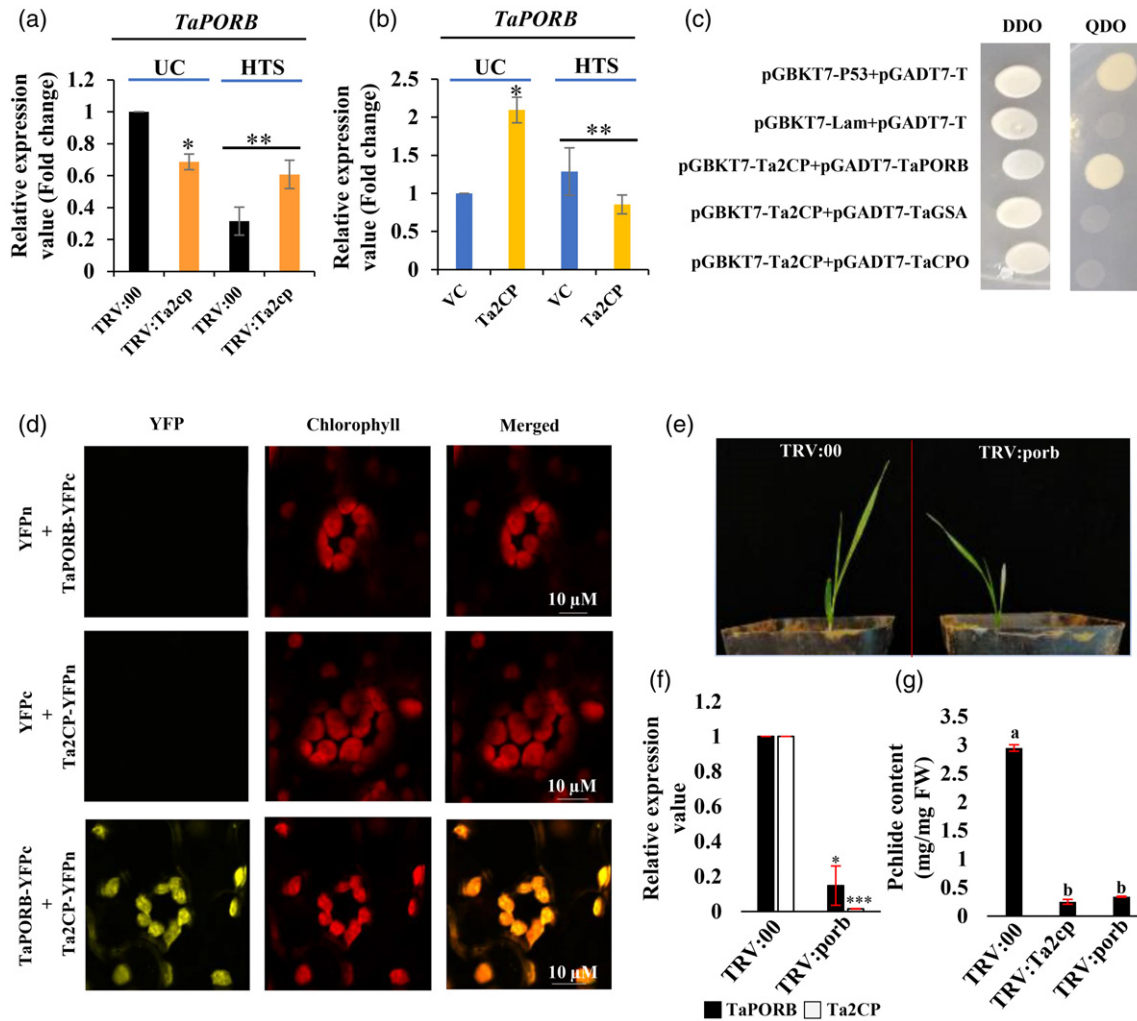
Figure 4. Coordinated role of Ta2CP and TaPORB.

(a,b) Relative abundance of *TaPORB* transcripts in Ta2cp-silenced and Ta2CP-overexpressed plants. Single asterisk denotes statistical significance relative to their corresponding TRV:00/vector control (VC; Student's *t*-test), while double asterisks denote significant differences between TRV:00/VC and silenced/overexpressed plants (two-way ANOVA) upon exposure to high-temperature stress (HTS; ** $P < 0.05$). Data shown are means ± SE of three replicates.

(c) Pair-wise yeast-two-hybrid (Y2H) interactions of Ta2CP with TaPORB, TaCPO and TaGSA on DDO and QDO plates. Yeast cultures for positive (pGBKT7-p53 with pGADT7-T) and negative (pGBKT7-Lam with pGADT7-T) controls were also plated on QDO media. Double dropout, DDO; Quadruple dropout, QDO.

(d) *In planta* interactions of Ta2CP with TaPORB by co-transforming Ta2CP-YFPn and TaPORB-YFPc into *Nicotiana benthamiana* leaves. The plasmids YFPn with TaPORB-YFPc and Ta2CP-YFPn with YFPc were used as negative control. Scale bar: 10 μm.

(e) Representative images showing morphological phenotypes of Taporb-silenced plants and VC (TRV:00).

(f) Bar graphs showing relative abundance of *TaPORB* and *Ta2CP* transcripts in Taporb-silenced plants with reference to TRV:00.

(g) Accumulation of protochlorophyllide in TRV:00, Ta2cp-silenced plants and Taporb-silenced plants. The protochlorophyllide is expressed as mg per mg fresh weight, Pchlide, protochlorophyllide. The experiments were performed in triplicate and statistical significance relative to TRV:00 (Student's *t*-test, ***$P < 0.001$ and *$P < 0.05$).

regulated by redox-dependent ADP-glucose pyrophosphorylase (AGPase) activation (Hou *et al.*, 2019). Hence, we sought to understand the role of Ta2CP in controlling starch accumulation. Interestingly, Ta2cp-silenced and -overexpressed plants showed high and low starch content, respectively (Figure 5a,b). To find a possible explanation, we quantified the transcript abundance of the key regulator of starch biosynthesis, *AGPase*. The increase in *AGPase1* expression was observed in Ta2cp-silenced plants under unstressed and HTS conditions, while increased *AGPase2*

expression was seen only in plants under HTS (Figure 5c, d). Furthermore, the reduced expression of *AGPase1* and *AGPase2* was found in Ta2CP-overexpressed lines (Figure 5e,f).

Ta2CP stimulates antioxidative pathways and reduces oxidative stress

Because Prxs play a role in detoxifying H_2O_2 and lipid peroxides, and they are known to act with other peroxide-removing enzymes (Dietz, 2016), we therefore checked the
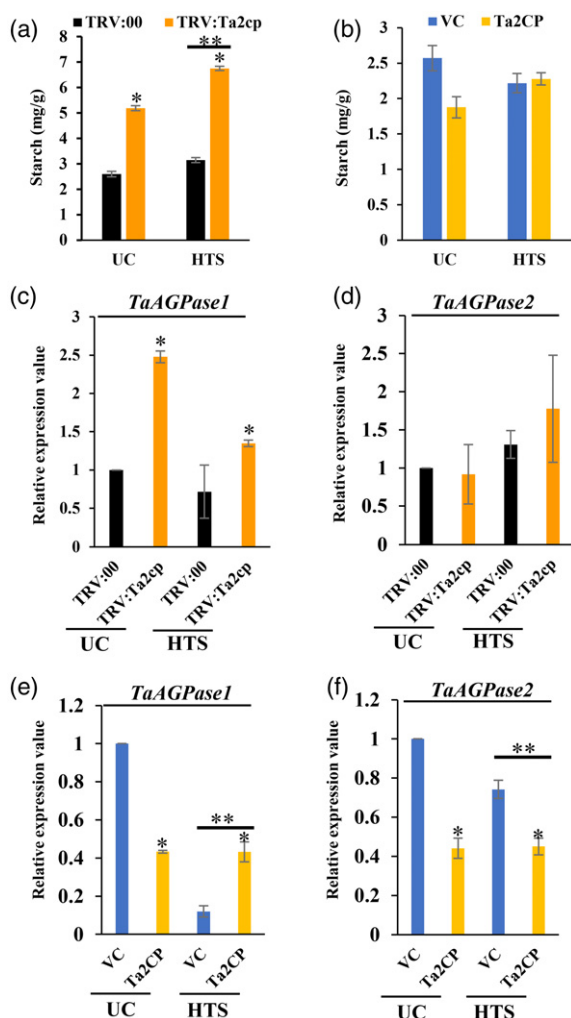
Figure 5. The role of Ta2CP on starch metabolism.

(a,b) Bar graphs indicate the starch content in Ta2cp-silenced and Ta2CP-overexpressed plants compared with TRV:00 and vector control (VC), respectively, under unstressed (UC) and high-temperature stress (HTS) conditions.

(c–f) Transcript abundance of *TaAGPase1* and *TaAGPase2* in (c,d) Ta2cp-silenced lines and (e,f) Ta2CP-overexpressed plants under UC and HTS conditions.

Single asterisk denotes significant differences relative to TRV:00/VC (Student's *t*-test), while double asterisks denote significant differences between TRV:00/VC and silenced/overexpressed plants upon exposure to HTS ($P < 0.05$; two-way ANOVA). Mean values $\pm$ SE are shown for three independent experiments. TRV:00, VC of TRV-mediated silencing; VC, vector control used for transient expression in wheat; UC, unstressed.

impact of silencing and overexpressing 2CP on the status of other peroxidases in Ta2cp-silenced/Ta2CP-overexpressed plants under unstressed and HTS conditions. An increased (~67%) peroxidase activity was detected in Ta2cp-silenced plants compared with that in the vector control (Figure S11a). Interestingly, the change in peroxidase activity in Ta2CP-overexpressed plants was negligible (~8%) under unstressed conditions, while the activity was

increased (~23%) under HTS conditions (Figure S11b). In general, peroxidase activity is attributed to APx and glutathione peroxidase (GPx) besides Prxs. Thus, to correlate the effect of silencing and overexpression of a Prx, *Ta2CP* on the transcript abundance of other peroxidases and Prxs, we analyzed the transcript abundance of peroxidases and Prxs in Ta2cp-silenced and overexpressed plants under unstressed and HTS conditions. Transcripts of peroxidases such as *PrxIIB*, *PrxIIF*, *APx7* and *GPx* (cytosol) were either upregulated or maintained at a steady state under unstressed conditions (Figure S11c). Also, there was increased expression of *TaPER1* (nucleus), *GPx* (cytosol), *TaPrxQ* (chloroplast) and *TaAPx2* (chloroplast) in HTS-treated Ta2cp-silenced plants (Figure S11c). Furthermore, the transcript abundance of *PrxIIB*, *PrxIIE*, *PER1*, *PrxIIF*, *PrxQ*, *APx7* and cytosolic *GPx* positively correlated with the increased peroxidase activity of HTS-treated Ta2CP-overexpressed plants (Figure S11d).

To dissect the role of Ta2CP in the maintenance of H_2O_2 abundance, we examined the redox status of Ta2cp-silenced and Ta2CP-overexpressed plants. The Ta2cp-silenced plants displayed higher abundance of H_2O_2 under HTS compared with Ta2CP-overexpressed plants, which was consistent with the increased abundance of ROS, particularly superoxide anions (Figure 6a). Contrastingly, Ta2CP-overexpressed plants had low concentrations of H_2O_2 and ROS compared with their vector control, suggesting a crucial role of 2CP in ROS homeostasis (Figure 6b). Notably, lipid peroxidation level was slightly increased in Ta2cp-silenced plants, but decreased in Ta2CP-overexpressed plants when challenged with HTS (Figure 6c,d). More significantly, despite HTS-induced higher abundance of ROS, the Ta2cp-silenced plants showed no significant increase in lipid peroxidation and cell death (Figures 6c and S12a), indicating other factors influencing cellular homeostasis. Next, we assessed the expression of apoptosis- (cell death suppressors and initiator) and autophagy-related genes to determine whether HTS conditions induce apoptosis or autophagic cell death. The expression of *ACD1*, *ACD2* and *LrgB* (cell death suppressors) was increased, while the expression of *EX1* (programmed cell death initiator) was reduced in HTS-treated Ta2cp-silenced plants. The transcripts of autophagy-related genes such as *ATG8h*, *ATG6F* and *ATG8A*, and cochaperone *ClpC1* were also upregulated under HTS (Figure 6e). In contrast, the Ta2CP-overexpressed plants showed reduced expression of both apoptosis- (except *ACD1*) and autophagy-related genes and no cell death under HTS (Figures 6f and S12b).

DISCUSSION

Crop plants adopt various strategies to combat HTS conditions at physicochemical and molecular levels. Therefore, we analyzed HTS-triggered alterations of morphophysiological traits coupled with intracellular changes in tolerant
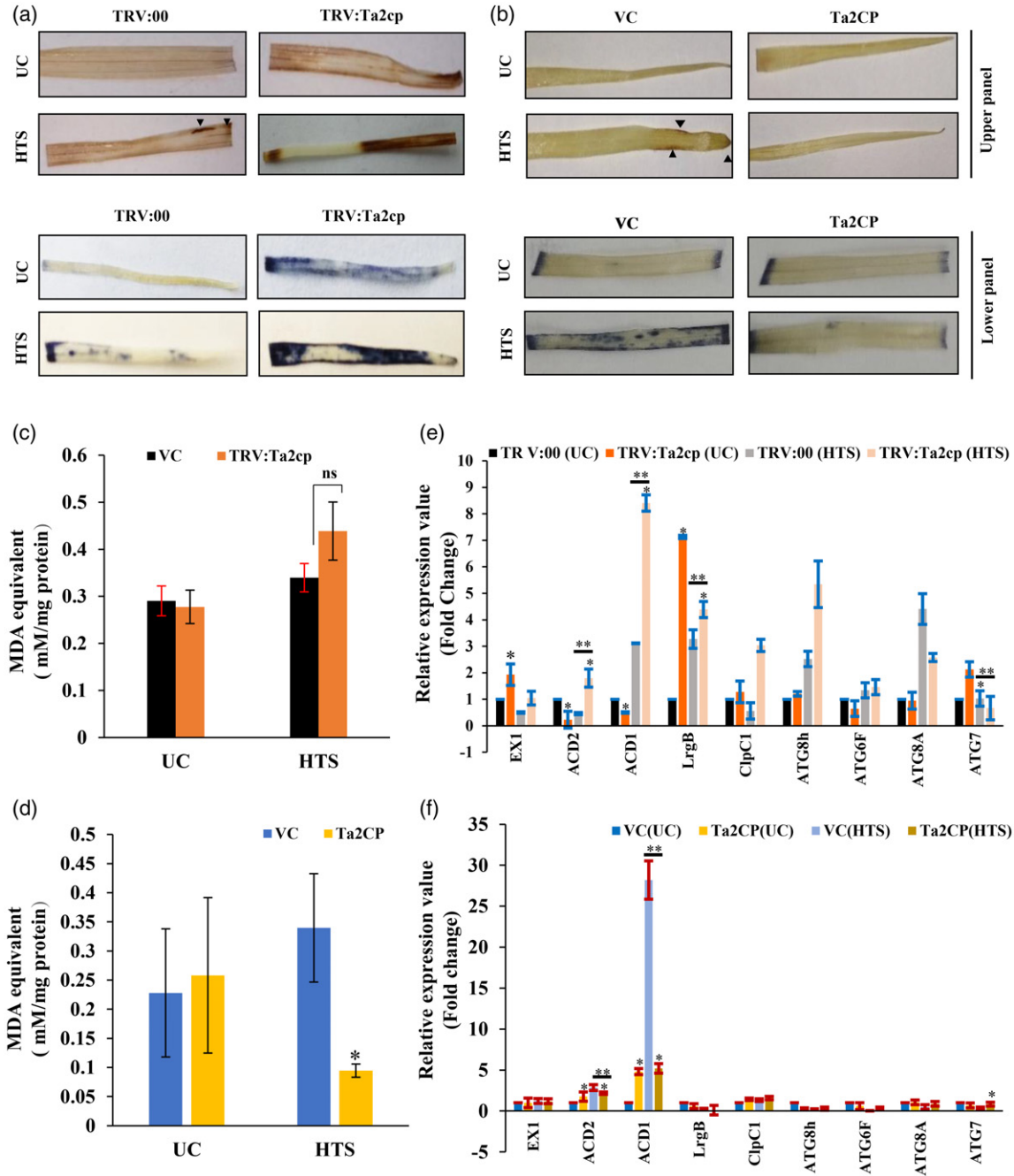
**Figure 6.** Role of Ta2CP in cell defense pathway.

(a,b) 3-Diaminobenzidine (DAB)-stained leaves showing H₂O₂ abundance (upper panel) and nitroblue tetrazolium (NBT)-stained leaves showing the abundance of superoxide anion (lower panel) in (a) Ta2cp-silenced and TRV:00, and (b) Ta2CP-overexpressed plants and vector control (VC) under unstressed (UC) and high-temperature stress (HTS) conditions.

(c,d) The quantitative determination of membrane damage in Ta2cp-silenced and Ta2CP-overexpressed plants under UC and HTS conditions. Membrane damage expressed as MDA equivalent (mM per mg protein) on the y-axis. ns, non-significant.

(e,f) Relative transcript abundance of autophagic- and apoptosis-related genes in (e) Ta2cp-silenced and (f) Ta2CP-overexpressed plants under unstressed and HTS conditions. Single asterisks denote significant differences relative to their corresponding TRV:00/VC ($P < 0.05$; Student's *t*-test), while doubled asterisks denote significant differences between TRV:00/VC and silenced/overexpressed plants in response to HTS ($P < 0.05$; two-way ANOVA). The experiments were conducted in triplicate and values are expressed as the means ± SE. TRV:00, VC of TRV-mediated silencing; VC, vector control used for transient expression in wheat.; UC, unstressed.

wheat U. Halna. Significant changes in physicochemical parameters were observed in advanced stages of HTS (Figure S1), which agrees with previous reports on stress-induced alterations in various crop species (Ma *et al.*, 2016). HTS-induced accumulation of soluble sugars and maintenance of antioxidant enzyme activity in early stages of HTS indicated that U. Halna is equipped with potential tolerance (Figures S1 and S6). To correlate the HTS-induced morpho-physicochemical traits with the proteome profile, we developed HTS-responsive cytoplasmic proteome, which revealed HRPs associated with Hsp-cochaperone, redox homeostasis, carbohydrate metabolism and photosynthesis as the key regulators of adaptive responses (Figures 1 and S2–S6; Tables S1 and S2). Previous studies have shown modulation of primary and secondary metabolites under stress, particularly HTS (Keunen *et al.*, 2013; Gayen *et al.*, 2019; Pareek *et al.*, 2019). Notably, higher accumulation of glutamic acid and alanine during HTS indicated the activation of GABA shunt, which has previously been shown to be activated by dehydration and salinity stress (Che-Othman *et al.*, 2019; Gayen *et al.*, 2019). As it is regulated via feedback control, the activity of GABA could be modulated with respect to the redox and energy status. This reconfiguration of energy metabolism (Figures 1d,e and S6; Table S4) provides a mechanistic insight into the adapted metabolic fingerprint of thermotolerance.

Complementation of *Ta2CP* in yeast and heterologous expression in Arabidopsis demonstrated its conserved stress-induced adaptive response across biological systems (Figure 2e–l). *In planta* characterization of Ta2CP indicated its role in growth and development. The Ta2cp-silenced plants showed a photobleaching-like phenotype coupled with altered leaf morphology and reduced plant height (Figures 3a and S8a–d). This agrees with previous studies reporting chlorosis in plants caused by mutations in 2CP (Vidigal *et al.*, 2014; Awad *et al.*, 2015; Cheng *et al.*, 2016), implying a key role in growth and development. Intriguingly, we also observed a photobleaching-like phenotype in few (< 25%) of the vector control plants, which might be due to the longer cocultivation period or high inoculum density of *Agrobacterium*, or both (Zhang *et al.*, 2017). The Ta2cp-silenced plants showed leaf wilting, curling and chlorosis when exposed to HTS, while Ta2CP-overexpressed plants remained unaffected (Figure 3a,b). Transcript analysis of *PORB* indicated that Ta2CP might function in the conversion of protochlorophyllide into chlorophyllide a, explaining why chlorophyll a was more vulnerable than chlorophyll b under HTS conditions in Ta2cp-silenced/Ta2CP-overexpressed plants (Figures 3c–f and 4a,b). We further demonstrated a physical interaction of Ta2CP with TaPORB, suggesting that this complex might be involved in the conversion of protochlorophyllide into chlorophyllide a (Figures 4c,d and 7a). Reciprocal downregulation of *Ta2CP* in Taporb-silenced and *TaPORB* in
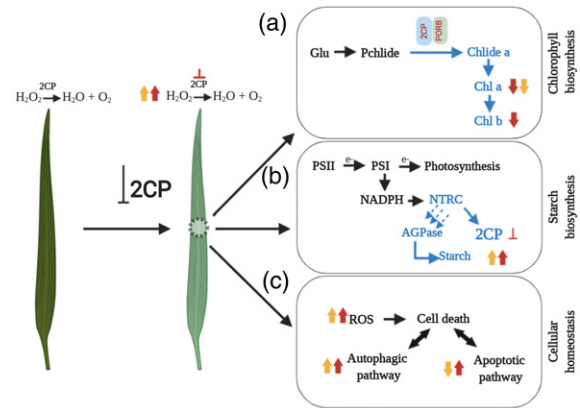
Figure 7. Predictive model of Ta2CP function in wheat. The phenotypic changes and its associated alterations at molecular level due to downregulation of Ta2CP.

(a) The penultimate reaction of chlorophyll biosynthesis is catalyzed by PORB. Interaction of TaPORB with Ta2CP plays an important role in conversion of protochlorophyllide to chlorophyllide a. Modulation in Ta2CP level affects the interaction and hence chlorophyll biosynthetic pathway.

(b) Downregulation of 2CP might enhance the interaction efficacy of NTRC with AGPase and stimulate starch biosynthesis.

(c) Ta2CP fine-tunes the autophagic and apoptotic pathways to maintain the cellular homeostatic system under extreme high-temperature stress (HTS) conditions. Red bold arrows indicate the effect of downregulation of Ta2CP under unstressed condition, while yellow bold arrows indicate the effect under HTS conditions. Glu, glutamic acid; Pchlide, protochlorophyllide; chllide, chlorophyllide; Chl a, chlorophyll a; Chl b, chlorophyll b; PS, photosystem; NTRC, NADPH-dependent Trx reductase C; AGPase, ADP-glucose pyrophosphorylase; ROS, reactive oxygen species (the figure was created with the help of BioRender.com).

Ta2cp-silenced plants indicate the importance of their collective role in maintaining the chlorophyll biosynthetic pathway (Figure 4a,f).

The increased starch accumulation in Ta2cp-silenced plants indicates the probable existence of an alternate regulatory mechanism for starch biosynthesis. AGPase is a key enzyme in the starch biosynthetic pathway that is regulated by NTRC (Michalska *et al.*, 2009). Interestingly, NTRC can efficiently reduce both 2CP and AGPase. Notably, the interaction between NTRC and AGPase has previously been reported to be relatively weaker than that between NTRC and 2CP (Lepistö *et al.*, 2013). Therefore, the interaction efficiency of AGPase with NTRC would be enhanced by silencing *Ta2CP* and thereby promoting activation of AGPase (Figures 5 and 7b). NTRC was primarily designated as the major modulator for the reduction of 2CP (Alkhalfioui *et al.*, 2006; Moon *et al.*, 2006; Pérez-Ruiz *et al.*, 2017). However, NTRC has been recognized as one of the regulators of photosynthesis, particularly under variable light conditions, and for the redox-regulation of enzymes associated in starch metabolism (Richter *et al.*, 2018). Also, the role of the NTRC/2CP system in the biosynthesis of protochlorophyllide has been established, as well as their role in H_2O_2 scavenging (Stenbaek *et al.*, 2008). We observed the

involvement of 2CP in the next step of conversion of protochlorophyllide to chlorophyllide a via its interaction with PORB, indicating that 2CP has a key role in regulation of the chlorophyll biosynthesis. Additionally, it has been evident that 2CP instigates the expression of different antioxidants during the development of early seedlings, and the reduced expression of 2CP induces photosynthetic inhibition (Baier and Dietz, 1999; Pena-Ahumada et al., 2006).

The presence of various peroxidases within a single cell, or even in a single subcellular compartment, indicates that these peroxidases work in a concerted manner to alleviate the impact of H_2O_2. Nevertheless, they differ on their electron donors and are associated with their unambiguous redox networks (Awad et al., 2015; Dietz, 2016). Different degrees of upregulation in Prxs and peroxidases in Ta2cp-silenced plants with or without HTS could possibly be the reason for increased peroxidase activity (Figure S11a,c). However, most peroxidases and Prx were found to be upregulated in HTS-treated Ta2CP-overexpressed plants (Figure S11d). These results suggest that the alteration in the abundance level of *Ta2CP* might alter the expression of other cellular peroxidases and Prx.

Ta2cp-silenced and -overexpressed plants displayed increased and decreased accumulation of H_2O_2 and ROS, respectively, when compared with their respective vector controls (Figure 6a,b). A previous report demonstrated that heat-stressed chloroplasts release ROS and induce apoptotic-like PCD (AL-PCD) (Doyle et al., 2010). It is, thus, likely that the knockdown of chloroplastic *Ta2CP* might induce the production of H_2O_2, leading to cellular damage under HTS. However, no significant difference in cellular damage was observed in HTS-treated Ta2cp-silenced plants when compared with HTS-treated vector control (Figures 6c and S12a), indicating that HTS-triggered increased ROS production in Ta2cp-silenced plants did not translate into activation of the apoptotic pathway. The increased expression of cell death suppressors in HTS-treated Ta2cp-silenced plants indicates that other factors might play a crucial role in maintaining cell viability. Notably, ACD1 and ACD2 stimulate the chlorophyll degradation pathway and help to regulate AL-PCD (Yao and Greenberg, 2006). Additionally, LrgB has previously been implicated in the inhibition of cell death and promotes chloroplast development. Interestingly, apart from the cell death suppressors, the plastid-localized cell death initiator *EX1* (Lee et al., 2007) was found to be downregulated. The reduction of *EX1* transcripts in HTS-treated Ta2cp-silenced plants reconfirmed the downregulation of AL-PCD (Figure 6e). These findings suggest that there must be an alternate mechanism that might control AL-PCD and maintain the Ta2cp-silenced plants under less severe HTS conditions (Figure 7c). As apoptosis is tightly regulated by autophagy (Yonekawa and Thorburn, 2013), the HTS-treated Ta2cp-silenced plants showed increased expression of autophagy-related genes

(Figures 6e and 7c). Previous investigations indicated that 2CP could function as chaperone machinery under stress conditions (Jang et al., 2004; Kim et al., 2009). HTS-induced accumulation of *ClpC1* indicates that the maintenance of chaperone machinery was overtaken by ClpC1 in Ta2cp-silenced plants (Figure 6e). Additionally, the downregulation of chloroplast component EX1, molecular chaperone ClpC1 and autophagy-related genes, as well as reduced cell death in Ta2CP-overexpressed plants suggest their concerted role in ROS mitigation. Additionally, the role of other control loops might also be postulated. These findings suggest that Ta2CP might initiate an adaptive process and provide protection against the consequences of severe stress.

In summary, HTS-responsive cytoplasmic proteome led to the identification of a Ta2CP with increased expression in due course of HTS, presumably involved in stress perception and adaptation. Furthermore, complementation of Ta2CP in yeast and heterologous expression in Arabidopsis demonstrated its role in thermotolerance. Both downregulation and overexpression of Ta2CP in wheat showed distinct developmental phenotypes, suggesting a role in plant growth and development. Silencing and overexpression of Ta2CP inferred involvement of 2CP in chlorophyll metabolism possibly via interaction with TaPORB.

EXPERIMENTAL PROCEDURES

Plant growth, maintenance and HTS-treatment

Seedlings of bread wheat (*Triticum aestivum* L. 'U. Halna') were grown in pots containing a mixture of soil and peat (3:1) in an environmentally controlled growth chamber at 23°C/18°C day/night temperature, 16 h photoperiod (350 μmol m^{-2} sec^{-1} light intensity) and 60 ± 5% relative humidity. Four-week-old seedlings were subjected to HTS conditions as previously described (Mishra et al., 2017). The aerial parts of unstressed control and those of HTS-treated seedlings were harvested, frozen in liquid nitrogen and stored at −80°C unless otherwise described.

Analysis of physicochemical indices

The accumulation of H_2O_2 and superoxide anion was detected using 3-diaminobenzidine (DAB) and nitroblue tetrazolium (NBT) staining, respectively, as previously described (Barua et al., 2018), and H_2O_2 concentrations were quantified as described earlier (Sergiev et al., 1997). Leaf tissues (300 mg) were homogenized in 0.1% (w/v) TCA, and the reaction was set by adding 10 mM KH_2PO_4 buffer (pH 7.0) and 1 M KI. The absorbance was read spectrophotometrically at 390 nm and expressed as μmol g^{-1} fresh weight.

Cell viability was determined by dipping the leaves in 0.25% (w/v) Evans blue and then vacuum infiltrated for 8 h. To quantify the staining, the leaves were homogenized in 1% (w/v) SDS at 50°C for 30 min, and absorbance was read spectrophotometrically at 600 nm.

Assessment of antioxidants, lipid peroxidation and soluble sugars

Leaf tissues (100 mg) were homogenized in 1 M phosphate buffer (pH 7.0), and the supernatant was used to analyze the

antioxidants. The spectrometric determination of APx, GR, POD and SOD activity was performed as described previously (Cakmak and Marschner,1992). Lipid peroxidation was estimated in terms of malondialdehyde (MDA) production as described earlier (Pareek *et al.*, 2019). Soluble sugars and starch were estimated using the standard anthrone method (Marshall, 1986).

Transmission electron microscopy visualization of intracellular changes

The leaves were incubated in Karnovsky's fixative solution [2% (v/v) paraformaldehyde and 2.5% (v/v) glutaraldehyde]. Samples were washed with 0.1 M phosphate buffer and treated with OsO_4. The leaves were dehydrated sequentially in acetone, placed in epoxy resin and thin sections were stained with uranyl acetate and lead citrate.

Isolation, enrichment and development of cytoplasmic proteome

Cytoplasmic proteins were isolated as previously described (Lim *et al.*, 2012) with few modifications. The aerial parts of seedlings were ground in liquid nitrogen with 0.3% (w/v) polyvinyl propylene (PVPP). The tissue powder was mixed in MOPS-KOH buffer (pH 7.5) and the slurry was centrifuged at 1500 *g* for 15 min at 4°C. The resulting supernatant was centrifuged at 16 500 *g* for 10 min at 4°C. The supernatant cytoplasmic fraction was precipitated with 10% (v/v) TCA overnight, and the pellet was washed with 80% (v/v) methanol, followed by 0.1 M ammonium acetate in methanol and 80% (v/v) acetone to remove the residual TCA. The pellet was resuspended in sucrose buffer [30% (w/v) sucrose, 0.1 M Tris-Cl pH 8.0, 5% (w/v) β-ME and 2% (w/v) SDS] and Tris-saturated phenol (v/v; 1:1 ratio) incubated at 25°C for 10 min, and centrifuged for 15 min at 16 500 *g*. The phenol phase was carefully retrieved in a microfuge tube, mixed with four volumes of 0.1 M ammonium acetate in methanol and incubated overnight at 4°C. The sample was then centrifuged, and the pellet obtained was resuspended in rehydration buffer [7 M urea, 2 M thiourea, 20 mM DTT and 4% (w/v) CHAPS] (Figure S2a). Protein concentration in the sample was quantified using a 2-DE Quant Kit (GE Healthcare, Piscataway, NJ, USA).

The validation of enriched cytoplasmic proteins was carried out using different organelle markers, such as anti-COX, anti-RbCL, anti-FBA, anti-XET and anti-PIP2. Densitometric analyses of immunoblots were performed using the Quantity One software (v. 4.1). The activity of alcohol dehydrogenase was determined spectrophotometrically. The reaction mixture contained 50 mM phosphate buffer, 3% (v/v) ethanol, 15 mM NAD and an optimized amount of cytoplasmic supernatant. The increase in absorbance was observed at 340 nm for 3 min, and the activity was calculated using the molar extinction coefficient 6.2 mM cm^{-1} (Figure S2b,c). The development of proteome, statistical analysis and identification of proteomic data were performed as described previously (Jaiswal *et al.*, 2013). The log2 fold values of proteins were used to construct the heat map in MeV software (http://www.tm4.org/mev.html).

Functional annotation of HTS-responsive proteome

The HRP sequences were used as a query against wheat protein sequence data available in the STRING database (v. 11.0; https://stringdb.org/n). The corresponding hits of HRPs and their interaction data were downloaded in MS-excel format. The blast hits were replaced by their corresponding wheat HRPs, and the interaction data were used as input in CytoScape (v. 3.4.0) (Table S3)

to construct the interaction network. The PCA using the fold values of HRPs was performed using XLSTAT (2014).

Comparative analysis of HTS-responsive metabolites

The metabolites of unstressed control and HTS-treated seedlings were extracted and subjected to gas chromatography-mass spectrometry (GC-MS) as described previously (Shekhar *et al.*, 2016b). A sample volume of 1 μl was injected in splitless mode into the GC-MS (Shimadzu GCMS-QP2010) equipped with an AOC-20i auto-sampler. The GC oven conditions were set as follows: isothermal heating at 70°C for 3 min to 250°C for 5 min, and final heating at 310°C for 1 min. Helium was used as the carrier gas at a flow rate of 1 ml min^{-1}, injection volume of 0.5 μl (split ratio of 10:1), and injector temperature at 250°C. The analysis was performed using an Elite-1 fused silica capillary column (30 mm × 0.25 mm ID × 1 μMdf) operating in electron impact mode at 70 eV. The mass spectra were taken at 70 eV and a scan interval of 0.5 sec with a scanning range of 40–600 m/z. Metabolites were analyzed and identified by comparing their mass spectra with that from the NIST and/or Wiley library. The abundance of individual metabolites was normalized against internal standards, ribitol (2 mg ml^{-1}) and 2-methyl-3-heptanone (1.424 μg μl^{-1}), as previously described (Shekhar *et al.*, 2016a).

Molecular cloning and characterization of *Ta2CP*

Full-length cDNA of *Ta2CP* (TraesCS2A02G297500) was amplified using gene-specific primers (Table S7) and cloned into the entry vector (pENTR-D-TOPO). The cDNA was subcloned into the destination vector (pEarleyGate101) and yeast expression vector (pYES-DEST52). The chloroplast fraction was isolated as described earlier (Lande *et al.*, 2017), and electrophoresed along with whole-cell extract, and probed with anti-RbCL, anti-COX, anti-LHC and anti-Ta2CP. Phylogenetic analysis of the Prx family and distribution of 2CPs in major lineages of land plants were performed as described previously (Mishra *et al.*, 2018). The phylogram was constructed using the MEGA6 software and visualized using Interactive Tree of Life (iTOL; v. 3).

Expression of *Ta2CP* in heterologous systems

Yeast mutants (*Δtsa1*, *Δtsa2* and *Δtsa1Δtsa2*) were transformed with empty pYES-DEST52 vectors and complemented by pYES-DEST52 harboring *Ta2CP* using the EZ-Yeast Transformation Kit (MP Biomedicals, Maharashtra, India). The starting optical density of overnight grown cultures of wild-type yeast strain BY4741, pYES-DEST52-transformed BY4741 (vector control), single mutants (*Δtsa1* and *Δtsa2*), double mutant (*Δtsa1Δtsa2*) and complemented strains (*Δtsa1:Ta2CP*, *Δtsa2:Ta2CP* and *Δtsa1Δtsa2:Ta2CP*) was set to 1 and diluted ranging from 10^0 to 10^{-4}. A drop (5 μl) of each culture was applied on YPD plates and incubated at 30°C (unstressed), 37°C (HTS) and 15°C (low-temperature stress; Mishra *et al.*, 2018). In a separate set of experiments, the cultures were grown on YPD plates independently supplemented with 0.5 M NaCl (hypersalinity; Piao *et al.*, 1999) and 1.2 M sorbitol (osmotic stress; Zhi *et al.*, 2013), and incubated at 30°C for 36 h. For oxidative stress, overnight-grown YPD culture was supplemented with 4 mM H_2O_2 for 30 min, and similar parameters were followed for spotting on YPD plates (Tran and Green, 2019).

To overexpress Ta2CP in Arabidopsis, expression vector (pEarleyGate101) harboring Ta2CP was introduced in Arabidopsis using the floral dip method (Zhang *et al.*, 2006). The transformants were selected through BASTA spraying. To analyze HTS response, 4-week-old seedlings were subjected to 42°C for 2 h.

VIGS of Ta2CP in wheat

The VIGS protocol was followed using the TRV system as described earlier (Zhang *et al.*, 2017; Verma *et al.*, 2020) with few modifications. A target 300-bp unique sequence of *Ta2CP* and 200-bp unique sequence of *TaPORB* were cloned into pTRV2. Phytoene desaturase (*PDS*) of wheat and tomato was used as a positive control to check the efficiency of VIGS experiment (Figure S8a,b).

Wheat seeds were kept on wet germination paper for 48 h in the dark at room temperature. The sprouted seeds were injured with a needle and then dropped in YEP media with an equimolar ratio of pTRV1:pTRV2-Ta2CP (1:1) supplemented with 3.3 mm cysteine, 100 µM acetosyringone and 2.5% (v/v) Tween-20. Injured seeds were *Agrobacterium*-infiltrated under vacuum for 30 sec and incubated at 28°C for 8–10 h. The seeds were washed with water at least 10–12 times to remove excessive *Agrobacterium*, and sown in a 10-cm diameter pot. An equimolar mixture of *Agrobacterium* strain harboring pTRV1 and pTRV2 vector (TRV:00) was used as a vector control. The transcript abundance was determined as described earlier (Shekhar *et al.*, 2015) using SYBR Green PCR kit (Applied Biosystems, Foster City, CA, USA). To analyze the HTS response, 12-day-old seedlings were subjected to 38°C for 5 h.

Vacuum-assisted *Agrobacterium*-mediated *Ta2CP* delivery in wheat

The transgene integration and expression in wheat was standardized using pBI121 harboring GUS as a reporter (Figure S9a,b) following a protocol described previously (Wu *et al.*, 2014). A single colony from a freshly streaked plate was used to inoculate in 5 ml LB media supplemented with kanamycin (50 mg l^{-1}) and rifampicin (25 mg l^{-1}). The primary culture was used to inoculate 500 ml LB media with 200 µm acetosyringone and grown at 28°C for 16 h. The culture was pelleted and resuspended in AB-MS-MES media to OD$_{600}$ of 1.

Two-day-old wheat germinated seeds were injured with a needle and subjected to vacuum infiltration with *Agrobacterium* suspension in AB-MS-MES media at 80 kPa for 1 h. *Agrobacterium* cells containing pBI121 vector were used as positive control, and those harboring pEarleyGate101 vectors were used as vector control (VC). The Ta2CP expression vector, pEarleyGate101:Ta2CP, was used to generate Ta2CP-overexpressed plants. Germinating seedlings were washed multiple times and placed in Hoagland solution. GUS expression was determined after 4 days with GUS staining at 37°C for 48 h. To analyze HTS response, 12-day-old seedlings were subjected to 38°C for 5 h.

Y2H, BiFC assay and confocal microscopy

The entry vector (pENTR-D-TOPO) harboring *Ta2CP* was subcloned into gateway compatible vector pGBKT7. Next, full-length ORF of *TaPORB, TaGSA* and *TaCPO* without stop codon was cloned into pENTR-D-TOPO, and subcloned into pGADT7. The constructs were co-transformed with Ta2CP into *Saccharomyces cerevisiae* strain AH109. The interaction was assessed by drop assay on SD/-Ade/-His/-Leu/-Trp plates. The controls for the positive (pGBKT7-53 and pGADT7-T) and negative interactions (pGBKT7-Lam and pGADT7-T) were also assayed on quadruple dropout (SD/-Ade/-His/-Leu/-Trp) plates. The plates were incubated at 30°C for 72 h.

In a separate set of experiments, the entry vector pENTR-D-TOPO harboring *Ta2CP* and *TaPORB* was subcloned into gateway-based BiFC vectors; pSITE-nEYFP-N, designated as pSITE-nEYFP-N:Ta2CP, and pSITE-nEYFP-C, designated as pSITE-nEYFP-C:TaPORB, respectively. Next, pSITE-nEYFP-N:Ta2CP, pSITE-nEYFP-C:TaPORB and gene silencing suppressor p19 were co-infiltrated into leaves of 6-week-old *Nicotiana benthamiana* plants. For control setup of BiFC assay, leaves were infiltrated with pSITE-nEYFP-N:Ta2CP::pSITE-nEYFP-C and pSITE-nEYFP-N::pSITE-nEYFP-C:TaPORB. The fluorescence signal intensities in BiFC were visualized by a confocal laser-scanning microscope (Leica TCS SP5).

Estimation of protochlorophyllide and chlorophyll

Total chlorophyll content was extracted from 100 mg fresh leaves in 80% acetone, and chlorophyll a and chlorophyll b contents were determined as described earlier (Mishra *et al.*, 2017). Protochlorophyllide was extracted in 80% acetone containing 0.1 N ammonium hydroxide at 4°C, and protochlorophyllide content was determined spectrometrically as described previously (Kwon *et al.*, 2017).

Statistical analysis

Statistical significance of HTS responses in U. Halna was analyzed by one-way ANOVA keeping $P < 0.05$, and data were expressed as mean $\pm$ SE. Furthermore, the *post hoc* treatment was performed in which pair-wise comparisons were made using Fisher-least significant difference (LSD) at $P < 0.05$. The Student's *t*-test was performed to observe significant difference in silenced/overexpressed plants relative to TRV:00/VC. Two-way ANOVA was used to find the significant differences between TRV:00/VC and silenced/overexpressed plants challenged with HTS ($P < 0.05$).

AUTHOR CONTRIBUTIONS

NC, DM, SS and SC designed the research; DM and SS performed the experiments; DM, SS, NC and SC analyzed data; and DM and NC wrote the article.

CONFLICT OF INTEREST

The authors declare no conflict of interest.

DATA AVAILABILITY STATEMENT

All relevant data can be found within the manuscript and its supporting materials.

SUPPORTING INFORMATION

Additional Supporting Information may be found in the online version of this article.

Figure S1. HTS-induced changes in morphophysiological and ultrastructural traits of wheat. (a,b) Phenotypic changes in 4-week-old seedlings and leaves. (c,d) Qualitative and quantitative assessment of H_2O_2 abundance and (e,f) cell death. (g–k) Bar graphs showing accumulation of (g) APx, (h) GR, (i) POX, (j) SOD and (k) soluble sugars in 4-week-old seedlings when challenged with HTS conditions. APx, ascorbate peroxidase; GR, glutathione reductase; POX, peroxidase; SOD, superoxide dismutase. The experiments were carried out in triplicate and values are expressed as the means ± SE. Different letters indicate the level of statistical significance at $P < 0.05$ (Fisher's LSD); the same letters are not significantly different with each other. UC represents unstressed control, and d-1, d-2, d-3 and d-4 represent HTS treatment durations. (l) TEM images showing cell architecture (I, II, scale bar: 2 μm); cell organelles, chloroplast (III, IV, scale bar: 100 nm) and mitochondria (V, VI, scale bar: 100 nm) at UC and d-4. Mc, mitochondrial cristae and Th, thylakoid membrane is shown by arrowheads.

Figure S2. Isolation and enrichment of cytoplasmic proteins. (a) The outline of the protocol for tissue fractionation and isolation of cytoplasmic protein (as detailed in Experimental Procedures section). (b) Enrichment of cytoplasmic proteins validated using different organelle-specific markers (COX, cytochrome c oxidase; FBA, fructose-1,6-bisphosphate aldolase; RbCL, RuBisCO L subunit; XET, xyloglucan endo-transglycosylase; PIP2, plasma membrane intrinsic protein 2). Bar graphs on the right represent corresponding band intensity. Bars marked with ***$P < 0.001$ and **$P < 0.01$ were significantly different. (c) Bar graphs showing activity of alcohol dehydrogenase in cytoplasmic fraction and pellet. (d) Representative 1-dimensional electrophoresis (1-DE) and 2-dimensional gel electrophoresis (2-DE) images showing cytoplasmic proteome profile. Reference molecular masses (Mw) are indicated in kDa on the left.

Figure S3. HTS-induced cytoplasmic proteome map. The cytoplasmic proteins were isolated from the seedlings from unstressed control and HTS-treated period. (a) An equal amount of protein from each time point was resolved by 2-DE. (b) Technical replicate gels ($n = 3$) for each stage were computationally integrated using PDQuest software to generate the primary matchsets. (c) The higher level matchset was created from the integration of primary matchsets for each time point. UC represents unstressed control, and d-1, d-2, d-3 and d-4 represent HTS treatment durations.

Figure S4. Correlation analysis of technical replicates of 2DE gels. Scatter plots depicting the correlation between technical replicates of 2-DE gels from unstressed control (UC) and HTS treatments (d-1 to d-4). The plots showed high correlation coefficient values (~0.8).

Figure S5. HTS-responsive comparative cytoplasmic proteome. Heat map represents the log2 transformed expression values of HRPs. The HRPs were annotated by IWGSC RefSeq v1.0 reference sequence (detailed information is provided in Tables S1 and S2). UC represents unstressed control, and d-1, d-2, d-3 and d-4 represent durations of HTS treatment.

Figure S6. Schematic of the HTS-response network in wheat. Overview of major pathways (glycolytic, redox homeostasis, chaperone and photosynthetic, among others) associated with the HTS responses. Yellow text represents wide-ranging physiological effects, while blue text represents change in metabolite and red text in proteome profiles. Ala, alanine; Val, valine; Ser, serine; Asp, aspartic acid; Glu, glutamine; Gly, glycine; Thr, threonine.

Figure S7. Predictive interaction network of Ta2CP and phylogenetic analysis of Prxs. (a) Predictive interaction network of Ta2CP with wheat HRPs based on the previously reported experiment in Arabidopsis (Muthuramalingam *et al.*, 2009; Cerveau *et al.*, 2016).

(b) A cladogram depicting the number of Prxs and 2CP found in representative members of evolutionary lineage. The numerals in parentheses represent the number of Prx, and 2CP (Prx, 2CP). (c) The phylogenetic relationship of Prxs among the representative members of lower to higher plant species. Phylogram was constructed by the neighbor-joining method by keeping the bootstrap value 1000. The network was visualized by iTOL.

Figure S8. VIGS of Ta2cp in wheat and growth phenotype of silenced plants. (a) The representative images showing wild-type (WT), vector control (TRV:00) and Tapds (positive control; TRV:Tapds) under unstressed conditions. (b) Bar graph indicating the transcript abundance of *Ta2CP* in Ta2cp-silenced plants when compared with that in TRV:00. Values represent the means ± SE of five biological replicates with statistically significant differences (***$P < 0.001$). P1 and P2 are two regions from where primer pairs were constructed. (c) The representative photograph showing the height of TRV:00 and Ta2cp-silenced plants. (d) Bar graph showing differences in plant height of TRV:00 and Ta2cp-silenced plants. Values represent the means ± SE and asterisks indicate statistically significant differences (***$P < 0.001$). Different bars indicate the different values.

Figure S9. Transformation of wheat and phenotypic profiling of the transformants. (a) The representative images of GUS-stained pBI121 vector transformed plants. (b) Bar graphs showing transcript abundance of Ta2CP in Ta2CP-overexpressed wheat plants compared with VC. Values represent the means ± SE of three biological replicates. (c) Differences in plant height between VC and Ta2CP-overexpressed plants. (d) Bar graph showing plant height of Ta2CP-overexpressed plants with VC. Values represent the means ± SE of three independent experiments. Asterisks indicate statistically significant differences (*$P < 0.05$, ***$P < 0.001$). Different bars indicate the different values.

Figure S10. Relative transcript abundance of photosynthesis associated genes. Bar graphs showing changes in transcript abundance of (a,b) *TaCPO* and (c,d) *TaGSA* in Ta2cp-silenced and Ta2CP-overexpressed plants under UC and HTS-treated conditions. The values represent the means ± SE of three independent experiments. Single asterisk denotes significant differences relative to TRV:00/VC (Student's *t*-test), while double asterisks denote significant differences ($P < 0.05$) between TRV:00/VC and silenced/overexpressed plants in response to HTS (two-way ANOVA).

Figure S11. Effect of Ta2CP on cellular peroxidation. (a,b) Bar graphs showing peroxidase activity in (a) Ta2cp-silenced and (b) Ta2CP-overexpressed plants along with TRV:00 and VC, respectively, under UC and HTS conditions. (c,d) Relative transcript abundance of Prxs and peroxidase in (c) Ta2cp-silenced and (d) Ta2CP-overexpressed plants under UC and HTS conditions. Single asterisk denotes significant differences relative to TRV:00/VC (Student's *t*-test), while double asterisks denote significant differences between TRV:00/VC and silenced/overexpressed plants in response to HTS ($P < 0.05$; two-way ANOVA). The values represent means ± SE of three independent experiments. TRV:00, VC of TRV-mediated silencing; VC, vector control used for transient expression in wheat; UC, unstressed.

Figure S12. Cell death in Ta2cp-silenced and Ta2CP-overexpressed plants during HTS. (a,b) Evans blue staining of leaves indicates relative cell death in (a) Ta2cp-silenced and (b) Ta2CP-overexpressed plants with TRV:00 and VC, respectively, under UC and HTS condition. TRV:00, VC of TRV-mediated silencing; VC, vector control used for transient expression in wheat; UC, unstressed.

Table S1. Identification of HRPs

Table S2. The description of peptide information of identified HRPs through LC-MS/MS analysis

Table S3. Detailed list of interacting partners of HRPs in HTS-responsive proteome

Table S4. Non-redundant list of metabolites

Table S5. A description of a putative interactive partner of Ta2CP from HTS-responsive proteome

Table S6. Genome-wide analysis of Prx members in different plant species

Table S7. Detailed list of primers used in this study

REFERENCES

Alkhalfioui, F., Renard, M. and Montrichard, F. (2006) Unique properties of NADP-thioredoxin reductase C in legumes. *J. Exp. Bot.* **58**, 969–978.

Asseng, S., Ewert, F., Martre, P. *et al.* (2014) Rising temperatures reduce global wheat production. *Nat. Clim. Change*, **5**, 143–147.

Awad, J., Stotz, H.U., Fekete, A., Krischke, M., Engert, C., Havaux, M., Berger, S. and Mueller, M.J. (2015) 2-cysteine peroxiredoxins and thylakoid ascorbate peroxidase create a water-water cycle that is essential to protect the photosynthetic apparatus under high light stress conditions. *Plant Physiol.* **167**, 1592–1603.

Baier, M. and Dietz, K.-J. (1999) Protective function of chloroplast 2-cysteine peroxiredoxin in photosynthesis. Evidence from transgenic Arabidopsis. *Plant Physiol.* **119**, 1407–1414.

Barua, P., Lande, N.V., Subba, P., Gayen, D., Pinto, S., Keshava Prasad, T.S., Chakraborty, S. and Chakraborty, N. (2018) Dehydration-responsive nuclear proteome landscape of chickpea (*Cicer arietinum* L.) reveals phosphorylation-mediated regulation of stress response. *Plant Cell Environ.* **42**, 230–244.

Broin, M. and Rey, P. (2003) The plastidic 2-cysteine peroxiredoxin is a target for a thioredoxin involved in the protection of the photosynthetic apparatus against oxidative stress. *Plant Physiol.* **132**, 1335–1343.

Cakmak, I. and Marschner, H. (1992) Magnesium deficiency and high light intensity enhance activities of superoxide dismutase, ascorbate peroxidase, and glutathione reductase in bean leaves. *Plant Physiol.* **98**, 1222–1227.

Cerveau, D., Henri, P., Blanchard, L. and Rey, P. (2019) Variability in the redox status of plant 2-Cys peroxiredoxins in relation to species and light cycle. *J. Exp. Bot.* **70**, 5003–5016.

Cerveau, D., Kraut, A., Stotz, H.U., Mueller, M.J., Couté, Y. and Rey, P. (2016) Characterization of the *Arabidopsis thaliana* 2-Cys peroxiredoxin interactome. *Plant Sci.* **252**, 30–41.

Chauhan, H., Khurana, N., Tyagi, A.K., Khurana, J.P. and Khurana, P. (2011) Identification and characterization of high temperature stress responsive genes in bread wheat (*Triticum aestivum* L.) and their regulation at various stages of development. *Plant Mol. Biol.* **75**, 35–51.

Che-Othman, M.H., Jacoby, R.P., Millar, A.H. and Taylor, N.L. (2019) Wheat mitochondrial respiration shifts tricarboxylic acid cycle to the GABA shunt under salt stress. *New Phytol.* **225**, 1166–1180.

Cheng, F., Yin, L.L., Zhou, J., Xia, X.J., Shi, K., Yu, J.Q., Zhou, Y.H. and Foyer, C.H. (2016) Interactions between 2-Cys peroxiredoxins and ascorbate in autophagosome formation during the heat stress response in *Solanum lycopersicum*. *J. Exp. Bot.* **67**, 1919–1933.

Dietz, K.J. (2011) Peroxiredoxins in plants and cyanobacteria. *Antioxid. Redox Signal.* **15**, 1129–1159.

Dietz, K.J. (2016) Thiol-based peroxidases and ascorbate peroxidases: why plants rely on multiple peroxidase systems in the photosynthesizing chloroplast? *Mol. Cells*, **39**, 20–25.

Doyle, S.M., Diamond, M. and McCabe, P.F. (2010) Chloroplast and reactive oxygen species involvement in apoptotic-like programmed cell death in *Arabidopsis* suspension cultures. *J. Exp. Bot.* **61**, 473–482.

Gayen, D., Barua, P., Lande, N.V., Varshney, S., Sengupta, S., Chakraborty, S. and Chakraborty, N. (2019) Dehydration-responsive alterations in the chloroplast proteome and cell metabolomic profile of rice reveals key stress adaptation responses. *Environ. Exp. Bot.* **160**, 12–24.

Horling, F., König, J., Dietz, K.J. and Baier, M. (2002) The function of the chloroplast 2-cysteine peroxiredoxin in peroxide detoxification and its regulation. *J. Exp. Bot.* **53**, 1321–1329.

Hou, L.-Y., Ehrlich, M., Thormählen, I., Lehmann, M., Krahnert, I., Obata, T., Cejudo, F.J., Fernie, A.R. and Geigenberger, P. (2019) NTRC plays a crucial role in starch metabolism, redox balance, and tomato fruit growth. *Plant Physiol.* **181**, 976–992.

IPCC. (2018) Global warming of 1.5°C. In *An IPCC Special Report on the Impacts of Global Warming of 1.5°C above Pre-Industrial Levels and Related Global Greenhouse Gas Emission Pathways, in the Context of Strengthening the Global Response to the Threat of Climate Change, Sustainable Development, and Efforts to Eradicate Poverty* (Masson-Delmotte, V., Zhai, P., Pörtner, H.O., Roberts, D., Skea, J., Shukla, P.R., Pirani, A., Moufouma-Okia, W., Péan, C., Pidcock, R., Connors, S., Matthews, J.B.R., Chen, Y., Zhou, X., Gomis, M.I., Lonnoy, E., Maycock, T., Tignor, M. and Waterfield, T., eds). Geneva, Switzerland: World Meteorological Organization.

Jaiswal, D.K., Ray, D., Choudhary, M.K., Subba, P., Kumar, A., Verma, J., Kumar, R., Datta, A., Chakraborty, S. and Chakraborty, N. (2013) Comparative proteomics of dehydration response in the rice nucleus: new insights into the molecular basis of genotype-specific adaptation. *Proteomics*, **13**, 3478–3497.

Jang, H.H., Lee, K.O., Chi, Y.H. *et al.* (2004) Two enzymes in one: two yeast peroxiredoxins display oxidative stress-dependent switching from a peroxidase to a molecular chaperone function. *Cell*, **117**, 625–635.

Keunen, E.L.S., Peshev, D., Vangromsveld, J., Van Den Ende, W. and Cuypers, A. (2013) Plant sugars are crucial players in the oxidative challenge during abiotic stress: extending the traditional concept. *Plant Cell Environ.* **36**, 1242–1255.

Kim, J.M., To, T.K., Ishida, J., Morosawa, T., Kawashima, M. and Matsui, A. (2008) Alterations of lysine modifications on the histone H3 N-tail under drought stress conditions in *Arabidopsis thaliana*. *Plant Cell Physiol.* **49**, 1580–1588.

Kim, S.Y., Jang, H.H., Lee, J.R. *et al.* (2009) Oligomerization and chaperone activity of a plant 2-Cys peroxiredoxin in response to oxidative stress. *Plant Sci.* **177**, 227–232.

Kirchsteiger, K., Pulido, P., González, M. and Cejudo, F.J. (2009) NADPH Thioredoxin reductase C controls the redox status of chloroplast 2-Cys peroxiredoxins in *Arabidopsis thaliana*. *Mol. Plant*, **2**, 298–307.

König, J., Baier, M., Horling, F., Kahmann, U., Harris, G., Schürmann, P. and Dietz, K.-J. (2002) The plant-specific function of 2-Cys peroxiredoxin-mediated detoxification of peroxides in the redox-hierarchy of photosynthetic electron flux. *Proc. Natl. Acad. Sci.* **99**, 5738–5743.

Kwon, C.-T., Kim, S.-H., Song, G., Kim, D. and Paek, N.-C. (2017) Two NADPH: Protochlorophyllide Oxidoreductase (POR) isoforms play distinct roles in environmental adaptation in rice. *Rice*, **10**, 1.

Lande, N.V., Subba, P., Barua, P., Gayen, D., Keshava Prasad, T.S., Chakraborty, S. and Chakraborty, N. (2017) Dissecting the chloroplast proteome of chickpea (*Cicer arietinum* L.) provides new insights into classical and non-classical functions. *J. Proteomics*, **165**, 11–20.

Lee, K.P., Kim, C., Landgraf, F. and Apel, K. (2007) EXECUTER1- and EXECUTER2-dependent transfer of stress-related signals from the plastid to the nucleus of *Arabidopsis thaliana*. *Proc. Natl Acad. Sci. USA*, **104**, 10270–10275.

Lepistö, A., Pakula, E., Toivola, J., Rintamäki, E., Krieger-Liszkay, A. and Vignols, F. (2013) Deletion of chloroplast NADPH-dependent thioredoxin reductase results in inability to regulate starch synthesis and causes stunted growth under short-day photoperiods. *J. Exp. Bot.* **64**, 3843–3854.

Liebthal, M., Maynard, D. and Dietz, K.J. (2018) Peroxiredoxins and redox signaling in plants. *Antioxid. Redox Signal.* **28**, 609–624.

Lim, S., Chisholm, K., Coffin, R.H., Peters, R.D., Al-Mughrabi, K.I., Wang-Pruski, G. and Pinto, D.M. (2012) Protein profiling in potato (*Solanum tuberosum* L.) leaf tissues by differential centrifugation. *J. Proteome Res.* **11**, 2594–2601.

Liu, G., Zha, Z., Cai, H. *et al.* (2020) Dynamic transcriptome analysis of anther response to heat stress during anthesis in thermotolerant rice (*Oryza sativa* L.). *Int. J. Mol. Sci.* **21**, 1155.

Ma, C., Cao, J., Li, J., Zhou, B., Tang, J. and Miao, A. (2016) Phenotypic, histological and proteomic analyses reveal multiple differences associated with chloroplast development in yellow and variegated variants from *Camellia sinensis*. *Sci. Rep.* **6**, 33369.

Marshall, J.D. (1986) Drought and shade interact to cause fine-root mortality in Douglas-fir seedlings. *Plant Soil*, **91**, 51–60.

Michalska, J., Zauber, H., Buchanan, B.B., Cejudo, F.J. and Geigenberger, P. (2009) NTRC links built-in thioredoxin to light and sucrose in regulating

starch synthesis in chloroplasts and amyloplasts. *Proc. Natl Acad. Sci. USA*, **106**, 9908–9913.

Mishra, D., Shekhar, S., Agrawal, L., Chakraborty, S. and Chakraborty, N. (2017) Cultivar-specific high temperature stress responses in bread wheat (*Triticum aestivum* L.) associated with physicochemical traits and defense pathways. *Food Chem.* **221**, 1077–1087.

Mishra, D., Shekhar, S., Chakraborty, S. and Chakraborty, N. (2018) Carboxylate clamp tetratricopeptide repeat (TPR) domain containing Hsp90 cochaperones in Triticeae: an insight into structural and functional diversification. *Environ. Exp. Bot.* **155**, 31–44.

Moon, J.C., Jang, H.H., Chae, H.B. *et al.* (2006) The C-type Arabidopsis thioredoxin reductase ANTR-C acts as an electron donor to 2-Cys peroxiredoxins in chloroplasts. *Biochem. Biophys. Res. Commun.* **348**, 478–484.

Muthuramalingam, M., Seidel, T., Laxa, M., Nunes de Miranda, S.M., Gärtner, F., Ströher, E., Kandlbinder, A. and Dietz, K.-J. (2009) Multiple redox and non-redox interactions define 2-cys peroxiredoxin as a regulatory hub in the chloroplast. *Mol. Plant*, **2**, 1273–1288.

Pareek, A., Rathi, D., Mishra, D., Chakraborty, S. and Chakraborty, N. (2019) Physiological plasticity to high temperature stress in chickpea: adaptive responses and variable tolerance. *Plant Sci.* **289**, 110258.

Pena-Ahumada, A., Kahmann, U., Dietz, K.-J. and Baier, M. (2006) Regulation of peroxiredoxin expression versus expression of Halliwell-Asada-Cycle enzymes during early seedling development of Arabidopsis thaliana. *Photosynth. Res.* **89**, 99–112.

Pérez-Ruiz, J.M., Naranjo, B., Ojeda, V., Guinea, M. and Cejudo, F.J. (2017) NTRC-dependent redox balance of 2-Cys peroxiredoxins is needed for optimal function of the photosynthetic apparatus. *Proc. Natl Acad. Sci. USA*, **114**, 12069–12074.

Piao, H.L., Pih, K.T., Lim, J.H., Kang, S.G., Jin, J.B., Kim, S.H. and Hwang, I. (1999) An Arabidopsis GSK3/shaggy-like gene that complements yeast salt stress-sensitive mutants is induced by NaCl and abscisic acid. *Plant Physiol.* **119**, 1527–1534.

Pulido, P., Spínola, M.C., Kirchsteiger, K., Guinea, M., Pascual, M.B., Sahrawy, M., Sandalio, L.M., Dietz, K.-J., González, M. and Cejudo, F.J. (2010) Functional analysis of the pathways for 2-Cys peroxiredoxin reduction in *Arabidopsis thaliana* chloroplasts. *J. Exp. Bot.* **61**, 4043–4054.

Richter, A.S., Pérez-Ruiz, J.M., Cejudo, F.J. and Grimm, B. (2018) Redox-control of chlorophyll biosynthesis mainly depends on thioredoxins. *FEBS Lett.* **592**, 3111–3115.

Sakuraba, Y., Rahman, M.L., Cho, S.-H., Kim, Y.-S., Koh, H.-J., Yoo, S.-C. and Paek, N.-C. (2013) The rice faded green leaf locus encodes protochlorophyllide oxidoreductase B and is essential for chlorophyll synthesis under high light conditions. *Plant J.* **74**, 122–133.

Schwanhäusser, B., Busse, D., Li, N., Dittmar, G., Schuchhardt, J., Wolf, J., Chen, W. and Selbach, M. (2011) Global quantification of mammalian gene expression control. *Nature*, **473**, 337–342.

Sergiev, I., Alexieva, V. and Karanov, E. (1997) Effect of spermine, atrazine and combination between them on some endogenous protective systems and stress markers in plants. *Compt. Rend. Acad. Bulg. Sci.* **51**, 121–124.

Shekhar, S., Agrawal, L., Mishra, D., Buragohain, A.K., Unnikrishnan, M., Mohan, C., Chakraborty, S. and Chakraborty, N. (2016a) Ectopic expression of amaranth seed storage albumin modulates photoassimilate transport and nutrient acquisition in sweetpotato. *Sci. Rep.* **6**, 25384.

Shekhar, S., Mishra, D., Buragohain, A.K., Chakraborty, S. and Chakraborty, N. (2015) Comparative analysis of phytochemicals and nutrient availability in two contrasting cultivars of sweet potato (*Ipomoea batatas* L.). *Food Chem.* **173**, 957–965.

Shekhar, S., Mishra, D., Gayali, S., Buragohain, A.K., Chakraborty, S. and Chakraborty, N. (2016b) Comparison of proteomic and metabolomic profiles of two contrasting ecotypes of sweetpotato (*Ipomoea batata* L.). *J. Proteomics*, **143**, 306–317.

Shi, J., Yan, B., Lou, X., Ma, H. and Ruan, S. (2017) Comparative transcriptome analysis reveals the transcriptional alterations in heat-resistant and heat-sensitive sweet maize (*Zea mays* L.) varieties under heat stress. *BMC Plant Biol.* **17**, 26.

Stenbaek, A., Hansson, A., Wulff, R.P., Hansson, M., Dietz, K.J. and Jensen, P.E. (2008) NADPH-dependent thioredoxin reductase and 2-Cys peroxiredoxins are needed for the protection of Mg–protoporphyrin monomethyl ester cyclase. *FEBS Lett.* **582**, 2773–2778.

Streward, F.C. (1942) The cytoplasm of the plant cell. *Nature*, **149**, 484–485.

Tran, K. and Green, E.M. (2019) Assessing yeast cell survival following hydrogen peroxide exposure. *Bio-protocol*, **9**, e3149.

Vaseghi, M.J., Chibani, K., Telman, W., Liebthal, M.F., Gerken, M., Schnitzer, H., Mueller, S.M. and Dietz, K.J. (2018) The chloroplast 2-cysteine peroxiredoxin functions as thioredoxin oxidase in redox regulation of chloroplast metabolism. *eLife*, **7**, e38194.

Verma, P.K., Verma, S., Tripathi, R.D. and Chakrabarty, D. (2020) A rice glutaredoxin regulate the expression of aquaporin genes and modulate root responses to provide arsenic tolerance. *Ecotoxicol. Environ. Saf.* **195**, 110471.

Vidigal, P., Martin-Hernandez, A.M., Guiu-Aragonés, C., Amâncio, S. and Carvalho, L. (2014) Selective silencing of 2Cys and type-IIB peroxiredoxins discloses their roles in cell redox state and stress signaling. *J. Integr. Plant Biol.* **57**, 591–601.

Weber, A.P.M. and Osteryoung, K.W. (2010) From endosymbiosis to synthetic photosynthetic life. *Plant Physiol.* **154**, 593–597.

Wong, C.-M., Siu, K.-L. and Jin, D.-Y. (2004) Peroxiredoxin-null yeast cells are hypersensitive to oxidative stress and are genomically unstable. *J. Biol. Chem.* **279**, 23207–23213.

Wu, H.Y., Liu, K.H., Wang, Y.C., Wu, J.F., Chiu, W.L., Chen, C.Y., Wu, S.H., Sheen, J. and Lai, E.M. (2014) AGROBEST: an efficient *Agrobacterium*-mediated transient expression method for versatile gene function analyses in *Arabidopsis* seedlings. *Plant Methods*, **10**, 19.

Yao, N. and Greenberg, J.T. (2006) Arabidopsis ACCELERATED CELL DEATH 2 modulates programmed cell death. *Plant Cell*, **18**, 397–411.

Yonekawa, T. and Thorburn, A. (2013) Autophagy and cell death. *Essays Biochem.* **55**, 105–117.

Zhang, N., Zhang, L., Zhao, L., Ren, Y., Cui, D., Chen, J., Wang, Y., Yu, P. and Chen, F. (2017) iTRAQ and virus-induced gene silencing revealed three proteins involved in cold response in bread wheat. *Sci. Rep.* **7**, 7524.

Zhang, X., Henriques, R., Lin, S.-S., Niu, Q.-W. and Chua, N.-H. (2006) *Agrobacterium*-mediated transformation of *Arabidopsis thaliana* using the floral dip method. *Nat. Protoc.* **1**, 641.

Zhi, H., Tang, L., Xia, Y. and Zhang, J. (2013) Ssk1p-independent activation of Ssk2p plays an important role in the osmotic stress response in saccharomyces cerevisiae: Alternative activation of Ssk2p in osmotic stress. *PLoS One*, **8**, e54867.